Chemical Science

ROYAL SOCIETY OF CHEMISTRY

EDGE ARTICLE

View Article Online
View Journal | View Issue

Check for updates

Cite this: *Chem. Sci.*, 2023, **14**, 14166

All publication charges for this article have been paid for by the Royal Society of Chemistry

Hydrogen spillover and substrate–support hydrogen bonding mediate hydrogenation of phenol catalyzed by palladium on reducible metal oxides†

Yeongseo An,‡[a] Puranjan Chatterjee,‡[ab] Pranjali Naik,[ab] Sayak Banerjee,[a] Wenyu Huang,[ab] Igor I. Slowing[ab] and Vincenzo Venditti *[ac]

Received 7th June 2023
Accepted 9th November 2023

DOI: 10.1039/d3sc02913a

rsc.li/chemical-science

Substrate–support interactions play an important role in the catalytic hydrogenation of phenolic compounds by ceria-supported palladium (Pd/CeO_2). Here, we combine surface contrast solution NMR methods and reaction kinetic assays to investigate the role of substrate–support interactions in phenol (PhOH) hydrogenation catalyzed by titania-supported palladium (Pd/TiO_2). We show that PhOH adsorbs on the catalyst *via* a weak hydrogen-bonding interaction between the –OH group of the substrate and one oxygen atom on the support. Interestingly, we observe that the addition of 20 mM inorganic phosphate results in a ~2-fold destabilization of the PhOH–support interaction and a corresponding ~2-fold inhibition of the catalytic reaction, suggesting an active role of the PhOH–TiO_2 hydrogen bond in catalysis. A comparison of the data measured here with the results previously reported for a Pd/CeO_2 catalyst indicates that the efficiency of the Pd-supported catalysts is correlated to the amount of PhOH hydrogen bonded to the metal oxide support. Since CeO_2 and TiO_2 have similar ability to uptake activated hydrogen from a noble metal site, these data suggest that hydrogen spillover is the main mechanism by which Pd-activated hydrogens are shuttled to the PhOH adsorbed on the surface of the support. Consistent with this hypothesis, Pd supported on a non-reducible metal oxide (silica) displays negligible hydrogenation activity. Therefore, we conclude that basic and reducible metal oxides are active supports for the efficient hydrogenation of phenolic compounds due to their ability to hydrogen bond to the substrate and mediate the addition of the activated hydrogens to the adsorbed aromatic ring.

Introduction

Phenolic compounds are high-volume petrochemicals currently employed in a myriad of industrial processes, from the production of polymer resins to the synthesis of pharmaceuticals.[1] In the past years, much effort has been made toward the development of strategies for the fundamental elaboration and diversification of phenols to unlock new routes for their conversion into higher-value chemicals.[1] In one of these applications, hydrogenation of phenol (PhOH) catalyzed by noble metals is used as an efficient route for large-scale production of cyclohexanone and cyclohexanol, which are important precursors for the synthesis of nylons and polyamide resins.[2] Recently, we have shown that Pd supported on ceria (Pd/CeO_2) can catalyze PhOH hydrogenation to cyclohexanone at room temperature and atmospheric pressure with unprecedented efficiency and selectivity.[3] In this catalyst, the supported Pd is required for H_2 adsorption and activation, while ceria mediates the adsorption of the small molecule into the catalytically competent substrate–catalyst adduct.[3–6] Although it is demonstrated that the hydrogen-bonding interaction between PhOH and ceria has a direct participation in catalysis,[4,5] it is unclear if the ability of ceria to mediate catalysis originates from its ability to shuttle the activated hydrogen to the substrate *via* hydrogen spillover, or to its capacity to facilitate constructive encounters between PhOH and Pd by optimizing the dispersion of the noble metal on the catalyst (Fig. 1). Similarly, it is not understood if other metal oxide supports can assist the hydrogenation reaction *via* analogous mechanisms.

Here we use surface contrast NMR (scNMR)[5,7] to investigate how the kinetics and thermodynamics of adsorption modulate the PhOH hydrogenation catalyzed by Pd supported on titania (Pd/TiO_2). Pd/TiO_2 has been previously shown to catalyze

[a]*Department of Chemistry, Iowa State University, Hach Hall, 2438 Pammel Drive, Ames, Iowa 50011, USA. E-mail: venditti@iastate.edu; Fax: +1-515-294-7550; Tel: +1-515-294-1044*

[b]*Department of Energy, Ames Laboratory, Ames, Iowa 50011, USA*

[c]*Roy J. Carver Department of Biochemistry, Biophysics and Molecular Biology, Iowa State University, Ames, Iowa 50011, USA*

† Electronic supplementary information (ESI) available. See DOI: https://doi.org/10.1039/d3sc02913a

‡ Equal contribution.

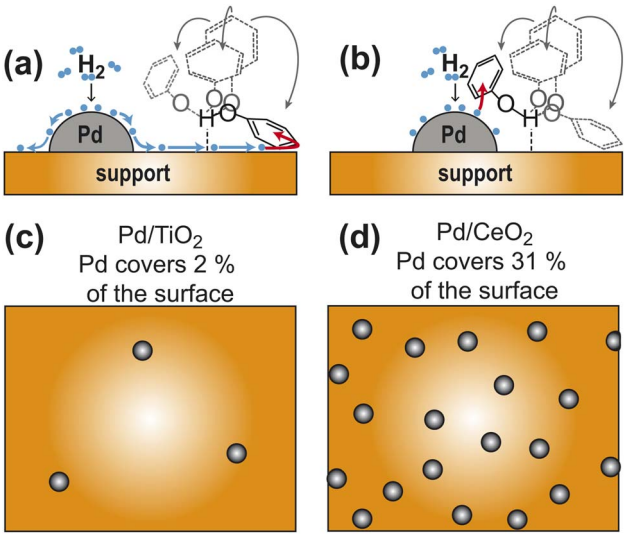

Fig. 1 Models for the participation of support in catalysis. (a) Pd-activated hydrogen spills over the support and reduces the aromatic ring of PhOH hydrogen bonded to the support. (b) Hydrogen bonding to the support facilitates the establishment of close contacts between PhOH and a nearby Pd site. Panels (c) and (d) are cartoon representations of a catalyst with a sparse and dense distribution of Pd sites, respectively. The ratio between metallic and support surface area has been chosen to correspond to the Pd/TiO_2 and Pd/CeO_2 catalysts in (c) and (d), respectively (see Table 1). In all panels the Pd sites are gray spheres and the support surface is an orange box. In panels (a) and (b) the activated hydrogens are blue spheres and four possible orientations of PhOH hydrogen bonded to the support are shown as formula structures. The PhOH orientation that receives hydrogen from the catalyst is colored black. The other three PhOH orientations are gray. Spillover is indicated by blue arrows. The addition of activated hydrogen to the aromatic ring is indicated by red arrows.

selective PhOH hydrogenation to cyclohexanone at mild temperature and pressure.[8,9] In this work, we use the Pd/TiO_2 catalyst to investigate the contribution of support–substrate interactions to catalysis. We show that the adsorption of PhOH on Pd/TiO_2 results in the formation of a weakly bound adduct in which the small molecule is likely hydrogen bonded to the support. In analogy to what we have previously observed for the Pd/CeO_2 catalyst,[5] we notice that the addition of 20 mM phosphate (at constant pH) results in a ~2-fold destabilization of the PhOH–titania interaction and in a corresponding ~2-fold reduction in catalytic conversion, which suggests that the weak substrate–support interaction is competent for the hydrogenation reaction catalyzed by Pd/TiO_2. Finally, a comparison of the data measured for the Pd/TiO_2 and Pd/CeO_2 catalysts indicates that, irrespective of the metal oxide, the kinetics of hydrogenation are correlated to the concentration of substrate hydrogen-bonded to the support. Since the ceria- and titania-based catalysts have drastically different Pd dispersion (Fig. 1) but a comparable ability to uptake activated hydrogen on the support surface,[10] our results indicate that hydrogen spillover is the main mechanism mediating catalytic conversion of PhOH hydrogen-bonded to the metal oxide support. Consistent with this conclusion, we show that silica-supported Pd (Pd/SiO_2) is incapable to mediate hydrogen spillover on the support and provides an inefficient catalyst for PhOH hydrogenation at mild conditions.

Results

Preparation of the Pd/TiO_2 catalyst

Titanium(IV) oxide, anatase nanopowder was purchased from Sigma-Aldrich and was used for catalyst preparation without further purification. In anatase TiO_2, the predominant crystallographic plane is (101), which is confirmed by the intense peak at $2\theta \sim 25°$ in the X-ray diffraction (XRD) pattern[11,12] (Fig. 2d). Pd nanoparticles were deposited on TiO_2 starting from the palladium(II) nitrate precursor *via* the incipient wetness impregnation method targeting 1 wt% Pd loading (see ESI Methods†). The XRD pattern of Pd/TiO_2 did not show the peak at $2\theta \sim 40°$ that is usually assigned to the (111) facet of the Pd nanoparticle[13] (Fig. 2d). This observation indicates that the deposited Pd particle size is below 3 nm. According to the transmission electron micrographs, the TiO_2 and Pd/TiO_2 particles are spherical in morphology with some irregularities (Fig. 2a and b).[14] The average size of 100 Pd/TiO_2 particles counted was 33 ± 8 nm (Fig. 2c), which is consistent with the claimed size of the commercial TiO_2 nanoparticles (~25 nm). N_2 sorption analysis reported a surface area of 76.0 $m^2\ g^{-1}$ for TiO_2 and 73.0 $m^2\ g^{-1}$ for Pd/TiO_2. The dispersion of the Pd nanoparticle was determined to be 38.5% by CO pulse chemisorption. The corresponding Pd particle size was ~2.7 nm. Given the metallic surface area of 1.6 $m^2\ g^{-1}$ obtained by CO pulse chemisorption,

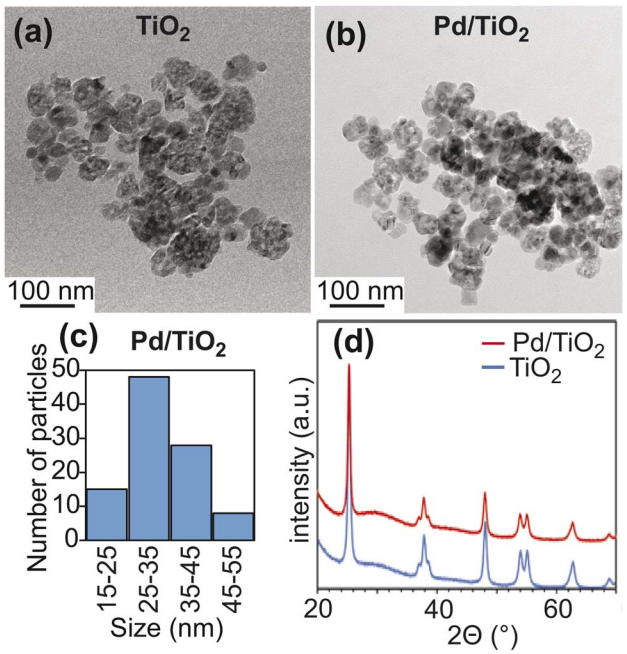

Fig. 2 Properties of TiO_2 and Pd/TiO_2. Panels (a) and (b) show TEM images for TiO_2 and Pd/TiO_2. Panel (c) shows a histogram of particle size constructed by counting 100 Pd/TiO_2 particles (average particle size 33 ± 8 nm). Panel (d) shows wide-angle PXRD patterns for TiO_2 (blue) and Pd/TiO_2 (red).

the actual TiO_2 surface area on the Pd/TiO_2 catalyst is calculated as 71.4 m^2 g^{-1} (73.0–1.6 m^2 g^{-1}) (Table 1).

Effect of TiO_2 and Pd/TiO_2 on PhOH ^{13}C transverse relaxation

In solution NMR, the interaction between an NMR-visible small molecule and an NMR-invisible nanoparticle can be conveniently detected by measuring the increase in ^{13}C transverse relaxation (R_2) of the small molecule upon addition of the nanoparticle (ΔR_2).[4,7,15] In the particular case of PhOH adsorption on a metal oxide particle, analysis of a plot of ΔR_2 *versus* the angle (θ) formed by the relevant ^{13}C–^{1}H bond and the *para* C–H bond provides thermodynamic and structural information on the adsorption process (Fig. 3). Indeed, we have previously shown that the formation of a hydrogen bond between the PhOH and the metal oxide surface generates a homogeneous increase in ^{13}C R_2 for the *ortho*, *meta*, and *para* positions that is the result of a homogeneous restriction of motion across the C–H bonds upon binding (Fig. 3a).[4,5] On the other hand, the interaction of PhOH with an oxygen vacancy on the nanoparticle selectively restricts the motion of the *para* C–H bond (Fig. 3b and d) and causes the ΔR_2 for the *para* carbon to be larger than the ΔR_2 values measured for the *ortho* and *meta* positions.[4,5,16] The data presented in Fig. 3e clearly indicate that the addition of 1 wt% TiO_2 to a 10 mM PhOH solution generates ΔR_2 values that are independent on θ (average $\Delta R_2 = 0.5 \pm 0.1$ s^{-1}). This observation indicates the absence (within the detection limit) of PhOH bound to oxygen vacancies and is consistent with the fact the titania is known to produce nanoparticles with a small number of defects.[17] Addition of 20 mM inorganic phosphate (Pi) to the sample at pH 7 (that matches the pH of the sample at 0 mM Pi, see ESI Methods†) results in a ~2-fold decrease in ΔR_2 (average $\Delta R_2 = 0.2 \pm 0.1$ s^{-1}) (Fig. 3e). Since Pi interacts strongly with metal oxide nanoparticles,[18] the observed reduction in ΔR_2 is a direct consequence of the competition between Pi and PhOH for the absorption sites and corroborates that the measured increase in R_2 reports on the PhOH–TiO_2 hydrogen-bonding interaction.

The ΔR_2 values measured upon addition of Pd/TiO_2 in the absence and in the presence of Pi (average $\Delta R_2 = 0.7 \pm 0.1$ and 0.2 ± 0.1 s^{-1}, respectively) are identical (within error) to the ones measured upon addition of TiO_2 (Fig. 3f), suggesting that deposition of Pd does not substantially affect the interaction between PhOH and the nanoparticle surface. This observation is consistent with the fact that deposition of Pd on the titania reduces the surface of the support slightly (from 76.0 to 71.4 m^2 g^{-1}) and that the metallic surface area (1.6 m^2 g^{-1}) is negligible compared to the support surface area in Pd/TiO_2 (Table 1). Finally, it is interesting to note that the ΔR_2 induced on PhOH by addition of 1 wt% Pd/TiO_2 is considerably smaller than the ΔR_2 previously measured in the presence of 1 wt% Pd/CeO_2 (average $\Delta R_2 = 1.6 \pm 0.1$ and 0.9 ± 0.1 s^{-1} in the absence and in the presence of 20 mM Pi, respectively) (Table 1),[5] which suggests that titania has lower affinity for PhOH than ceria.

scNMR characterization of PhOH adsorption on Pd/TiO_2

Further characterization of PhOH adsorption on Pd/TiO_2 was obtained by scNMR.[5,7] Three scNMR experiments were employed: dark-state saturation transfer (DEST), Carr–Purcell–Meiboom–Gill (CPMG) relaxation dispersion (RD), and longitudinal relaxation (R_1). The combined analysis of ^{13}C DEST, RD, and R_1 returns a comprehensive characterization of the thermodynamics and kinetics of adsorption processes occurring on the μs–s timescale, and provides structural information on the adsorbed species.[5,7]

The addition of 1 wt% TiO_2 or Pd/TiO_2 to a 10 mM solution of PhOH induces a homogeneous broadening of the DEST profiles and a shift to higher R_2 values of the RD curves measured for the *ortho*, *meta*, and *para* carbons of PhOH (ESI Fig. 1†), indicating the formation of a high molecular weight PhOH–nanoparticle adduct in chemical exchange with the free, NMR-visible small molecule.[7] The quantitative modeling of the experimental DEST, RD, and R_1 data was done using an adsorption/desorption exchange model in which all experimental observables are described by solutions to the McConnell equation (ESI Methods†). Analysis of the reduced χ^2 values obtained from modeling of the scNMR experiments indicates that all data can be accounted for by a two-site exchange kinetic model in which PhOH is in equilibrium between a desorbed (D) and an adsorbed (A) state (Fig. 4). The modeled parameters are shown in Fig. 5 and listed in ESI Tables S1 and S2.† Inspection of these

Table 1 Summary of the properties of the analyzed nanoparticles

	TiO_2	Pd/TiO_2	Pd/CeO_2[a]	Pd/SiO_2
Morphology	Spherical	Spherical	Cubic	Spherical
Diameter (nm)	33 ± 8	33 ± 8	25 ± 8	22 ± 5
BET surface area (m^2 g^{-1})	76.0	73.0	9.4	103.0
Metallic surface area (m^2 g^{-1})	—	1.6	2.9	1.4
Support surface area (m^2 g^{-1})	76.0	71.4	6.5	101.6
Cubic crystallite size (nm)	—	2.7	2.0	2.4
% dispersion	—	38	65	38
k (μM s^{-1}) @ 0 mM Pi	—	22.0 ± 0.2	30.5 ± 0.2	0
k (μM s^{-1}) @ 20 mM Pi	—	11.5 ± 0.2	15.7 ± 0.4	0
Aver. ^{13}C ΔR_2 (s^{-1}) @ 0 mM Pi[b]	0.5 ± 0.1	0.7 ± 0.1	1.6 ± 0.1	4.2 ± 0.1
Aver. ^{13}C ΔR_2 (s^{-1}) @ 20 mM Pi[b]	0.2 ± 0.1	0.2 ± 0.1	0.9 ± 0.1	2.6 ± 0.1

[a] Data on the Pd/CeO_2 catalyst were reported by Egner *et al.* (2020).[5] [b] ^{13}C ΔR_2 values averaged over the *ortho*, *meta*, and *para* positions.

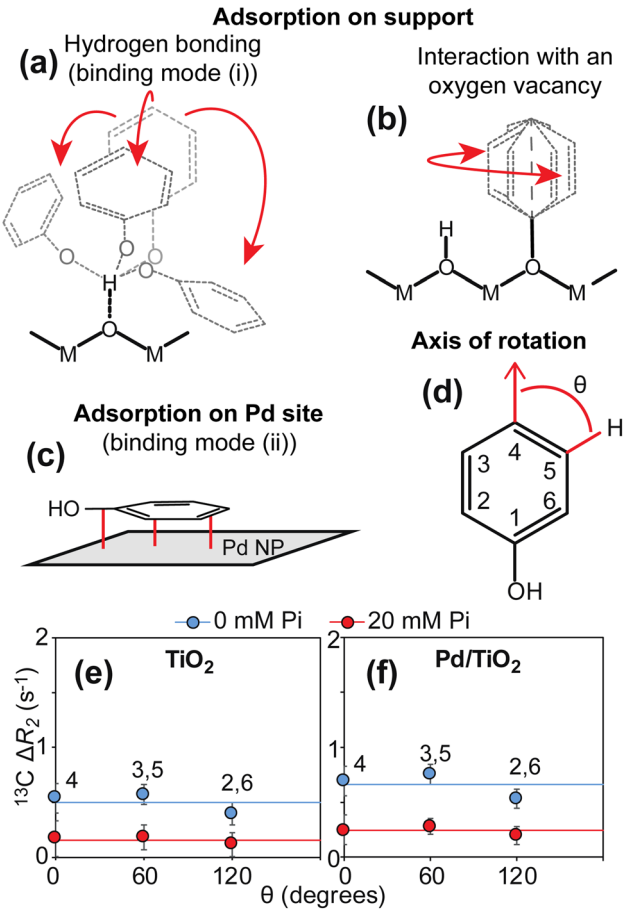

Fig. 3 ^{13}C ΔR_2 analysis. Panels (a–c) show the expected binding modes for PhOH on the surface of a nanoparticle formed by Pd supported on a metal oxide. In (a), PhOH is hydrogen bonded to the support. The motion of the three aromatic C–H bonds is restricted to a similar extent. In (b), PhOH is bound to an oxygen vacancy on the support. Only one rotatable bond separates the support from the aromatic ring. Therefore, the *para* C–H group appears static with respect to the axis of rotation. In (c), PhOH is rigidly adsorbed on the Pd site. All the aromatic C–H bonds tumble with the same correlation time as the nanoparticle (*i.e.* $S^2 \sim 1$).[5] M and O indicate the metal and oxygen atoms of the metal oxide, respectively. The Pd site is shown as a gray surface. Panel (d) shows the angle θ formed by the aromatic C–H bonds with the axis of rotation of a PhOH molecule bound to an oxygen vacancy. Panels (e) and (f) show a plot of the ^{13}C ΔR_2 as a function of θ measured for PhOH in the presence of 1 wt% TiO_2 and Pd/TiO_2, respectively. The *ortho* (2,6) and *meta* (3,5) positions generate equivalent NMR peaks and one single ΔR_2 value for these peaks is reported. Data measured in the presence of 0 and 20 mM Pi are shown as blue and red spheres, respectively. Solid blue and red lines are the corresponding average ΔR_2 values.

data reveals that the interaction between PhOH and TiO_2 is weak ($k_{AD} \sim 7700$ s^{-1} and population of adsorbed PhOH, p_A, ~1.0%) and confirms that dispersion of Pd on the nanoparticle surface does not significantly perturb the PhOH–nanoparticle interaction ($k_{AD} \sim 7400$ s^{-1} and $p_A \sim 1.2\%$) (Fig. 5a and b). On the other hand, the addition of 20 mM Pi to the solution results in a detectable destabilization of the interaction, which results in a ~2-fold reduction of the population of PhOH adsorbed to TiO_2 or Pd/TiO_2 ($p_A \sim 0.4$ and 0.6%, respectively). These results agree well with the ~2-fold decrease in ^{13}C ΔR_2 observed upon the addition of Pi (Fig. 3) and confirm that the detected PhOH–Pd/TiO_2 adduct involves interactions between the small molecule and titania that can be destabilized by the addition of Pi (note that Pi does not compete with PhOH for absorption on Pd).[5] This conclusion is further sported by the model-free (MF) analysis of the ^{13}C R_1 and R_2 rates obtained for the adsorbed state (see ESI Methods†). Indeed the MF analysis returns an order parameter (S^2) < 0.01 for the aromatic C–H groups of PhOH (Fig. 5), which is consistent with the order parameter expected for a PhOH molecule hydrogen bonded to a metal oxide nanoparticle,[5,16] and two orders of magnitude smaller than the S^2 expected for a PhOH molecule bound to the Pd site of Pd/TiO_2.[5] Finally, it is important to highlight that, while the scNMR data reported here do not provide evidence of a PhOH–Pd interaction in Pd/TiO_2, a prior scNMR study detected and characterized PhOH adsorption on Pd particles of ~2 nm size deposited on ceria nanocubes.[5] This apparent discrepancy is most likely the result of the lower metallic surface area in Pd/TiO_2 compared to Pd/CeO_2 (1.6 and 2.9 m^2 g^{-1}, respectively) (Table 1). Indeed, since the PhOH–Pd interaction detected on Pd/CeO_2 by DEST (population ~ 0.1%) was just above the detection limit of the experiment,[5] we expect the ~2-fold smaller metallic surface area in Pd/TiO_2 to further reduce the amount of PhOH adsorbed on the noble metal site and, therefore, push the PhOH–Pd adduct beyond the limit of detection.

Kinetics of PhOH hydrogenation by Pd/TiO_2

When multiple catalyst–support interaction modes are possible, the observed rate of a catalytic reaction is given by $k = \sum_i p_i k_i$, where p_i and k_i are the fractional abundance and turnover number of interaction mode i, respectively.[19–21] In the case of the PhOH hydrogenation reaction catalyzed by Pd/TiO_2, the two main binding modes at play are (i) PhOH hydrogen bonded to titania (detected by our scNMR experiments) and (ii) PhOH tightly adsorbed to the Pd site (below the detection limit of our scNMR experiments). To determine which binding mode is chiefly responsible for the catalytic conversion of PhOH, we have measured the rate of PhOH hydrogenation to cyclohexanone catalyzed by 1 wt% Pd/TiO_2 at pH 7.0, 35 °C, and 1 bar H_2 in the absence and the presence of 20 mM Pi. Since the addition of 20 mM Pi resulted in a ~2-fold reduction in binding mode (i) (Fig. 5) without affecting binding mode (ii),[5] we expect Pi to reduce catalytic conversion by ~50% if the reaction proceeds by binding mode (i) and to induce a negligible effect on k if the reaction proceeds by binding mode (ii) (Fig. 6a). Results presented in Fig. 6b indicate that the addition of 20 mM Pi to the reaction mixture reduces the rate of PhOH hydrogenation by ~2-fold (from 22.0 to 11.5 μM s^{-1}) (Table 1), clearly indicating that hydrogen bonding of PhOH to titania is chiefly responsible for the addition of the Pd-activated hydrogen on the aromatic molecule.

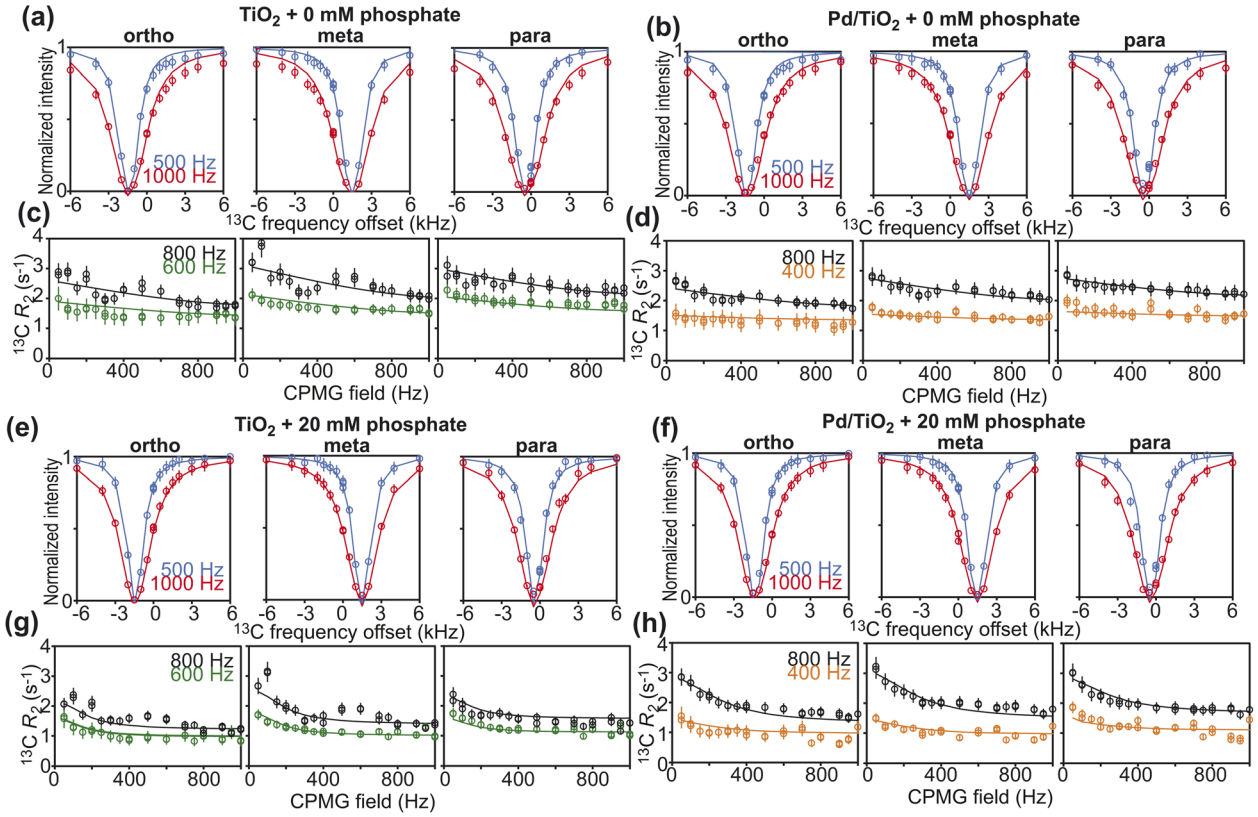

Fig. 4 scNMR analysis. ^{13}C DEST (top) and ^{13}C RD (bottom) profiles measured for the *ortho* (left), *meta* (center), and *para* (right) ^{13}C spins of PhOH in the presence of (a and c) 1 wt% TiO_2, (e and g) 1 wt% TiO_2 and 20 mM Pi, (b and d) 1 wt% Pd/TiO_2, and (f and h) 1 wt% Pd/TiO_2 and 20 mM Pi. ^{13}C DEST profiles were measured at saturation fields of 500 (blue) and 1000 (red) Hz. The R_2 rates for the RD profiles were acquired at 600 (green) and 800 (black) MHz for the TiO_2 data and 400 (orange) and 800 (black) MHz for the Pd/TiO_2 data. Experimental data are shown in circles, and the best-fit to a two-site exchange model are shown as solid lines. The agreement between experimental and back-calculated ^{13}C R_1 data is shown in ESI Fig. S2.† The fits return reduced χ^2 values of 1.4, 0.6, 0.6, and 1.0 for the TiO_2 and 0 mM Pi, TiO_2 and 20 mM Pi, Pd/TiO_2 and 0 mM Pi, and Pd/TiO_2 and 20 mM Pi, respectively.

Pd/TiO_2 *versus* Pd/CeO_2

Metal oxides are commonly used as supports for hydrogenation catalysts.[10] Therefore, understanding the mechanisms underlying the different performances of various metal oxide supports in hydrogenation reactions is of fundamental importance in catalysis science. We have investigated the performance of Pd/TiO_2 (this work) and Pd/CeO_2 (Egner *et al.* 2020)[5] as PhOH hydrogenation catalysts under identical experimental conditions (10 mM PhOH, 1 wt% catalysts, pH 7.0, 35 °C, and 1 bar H_2), and observed that Pd/CeO_2 catalyzes the reaction $\sim$ 1.5 times faster than Pd/TiO_2 (Table 1). Interestingly, by plotting the hydrogenation rate *versus* the concentration of PhOH weakly adsorbed on the support determined by scNMR experiments acquired in the absence and the presence of 20 mM Pi, it is apparent that the efficiency of the catalyst is correlated to the amount of the PhOH adsorbate, irrespective of the metal oxide used as the support (Fig. 6c). This observation indicates that the more pronounced basic properties of ceria compared to titania[17] enhance the affinity of the support for PhOH from 0.2 μmol m^{-2} in Pd/TiO_2 to 3.5 μmol m^{-2} in Pd/CeO_2 (calculated using the support surface areas from Table 1 and the concentrations of PhOH–support adduct in the absence of Pi from Fig. 6c) and make CeO_2 a better support for the hydrogenation reaction (note that PhOH acts as the hydrogen bond donor in its interaction with the metal oxide at pH 7.0 [4] and, therefore, it is expected to have a higher affinity for more basic surfaces).

In addition to revealing the basis for the outstanding performance of Pd/CeO_2 in catalytic hydrogenation of PhOH, our data suggest that hydrogen spillover is the main mechanism mediating the reduction of PhOH bound to the metal oxide support. Indeed, since ceria and titania have comparable abilities to uptake the Pd-activated hydrogen,[10] similar amounts of hydrogen atoms are expected to spillover onto the two supports, therefore resulting in the support-independent direct proportionality between catalytic efficiency and amount of PhOH adsorbed on the support observed in Fig. 6c. On the other hand, the correlation in Fig. 6c is inconsistent with the hypothesis that the better overall performance of the ceria-based catalyst is the result of a denser surface distribution of Pd sites that facilitates close encounters between the adsorbed PhOH and Pd on Pd/CeO_2 compared to Pd/TiO_2. Indeed, the latter hypothesis would suggest that Pd/CeO_2 catalyzes the reaction at a higher rate than Pd/TiO_2 when the same amount of PhOH is adsorbed on the support (note that a denser distribution of Pd sites increases the

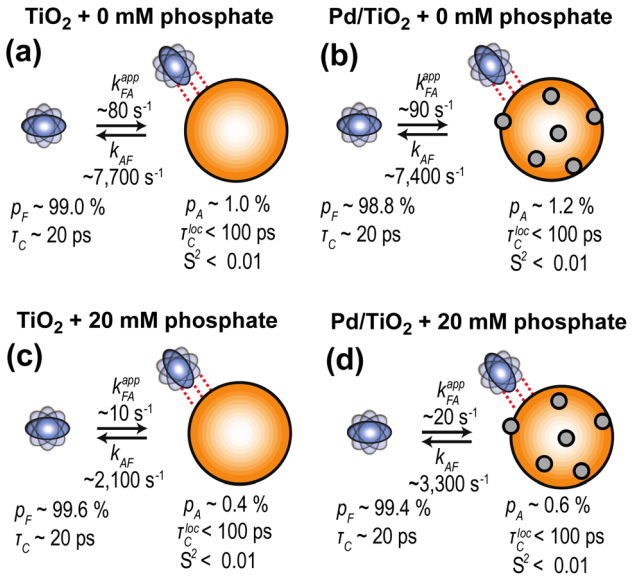

Fig. 5 Kinetic model for PhOH absorption on TiO_2 and Pd/TiO_2. Results of the simultaneous quantitative modeling of the ^{13}C DEST, RD, and R_1 data measured on 10 mM PhOH in the presence of (a) 1 wt% TiO_2, (b) 1 wt% Pd/TiO_2, (c) 1 wt% TiO_2, and 20 mM phosphate, and (d) 1 wt% Pd/TiO_2 and 20 mM phosphate. All data were interpreted using a two-site exchange model. TiO_2 is an orange sphere, and Pd NPs are gray spheres. PhOH is a blue rotating oblate. Dashed red lines indicate weak PhOH–nanoparticle interactions. Rate constants (k_{xy}, where x and y are the states in thermodynamic equilibrium; k_{xy}^{app} represents the apparent rate constant), populations of the two states (p_F and p_A for free and adsorbed states, respectively), the order parameter of the adsorbed state (S^2), and the rotational correlation time for local motion (τ_C^{loc}) were fit as global parameters. Chemical shift changes were fit as peak-specific parameters (see ESI Methods†). Best fit parameters are shown. A complete report of the fitted parameters is available in the ESI Tables S1 and S2.†

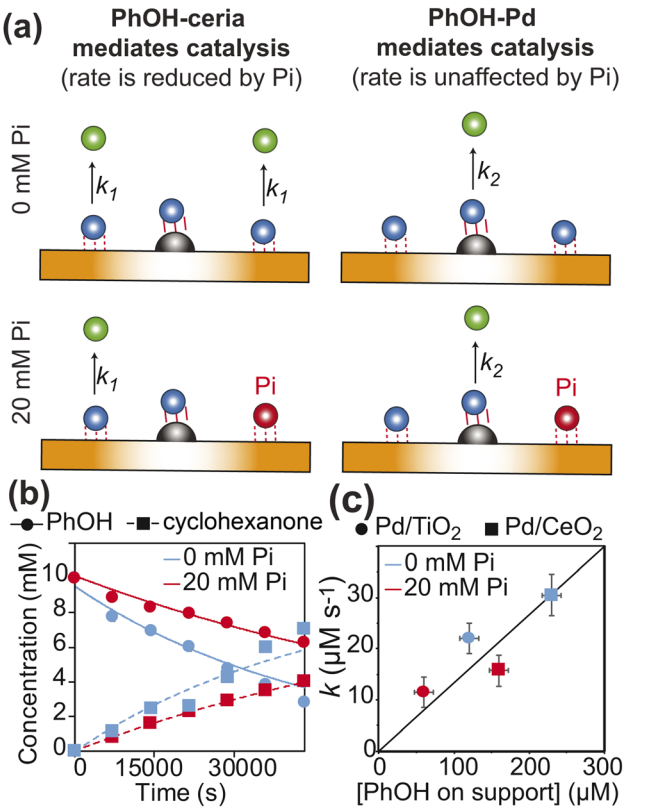

Fig. 6 Kinetics of PhOH hydrogenation. (a) Models of the dependence of the PhOH hydrogenation reaction from the concentration of inorganic phosphate (Pi). If the hydrogenation of PhOH proceeds from the substrate–support interaction with microscopic rate constant k_1 (left panel), a ~2-fold reduction of the PhOH–support interaction upon addition of 20 mM Pi results in a ~2-fold inhibition of the observed reaction rate $\left(k = \sum_i p_i k_i\right)$. If the reaction proceeds from the substrate–Pd adduct with microscopic rate constant k_2 (right panel), the addition of Pi is not expected to affect the observed rate of PhOH hydrogenation. PhOH, cyclohexanone, and Pi are represented as a blue, green, and red spheres, respectively. The Pd site is shown as a gray semi-sphere. The metal oxide support is shown as an orange surface. Red lines indicate the PhOH–catalyst interactions. (b) PhOH hydrogenation catalyzed by Pd/TiO_2 in the presence of 0 (blue) and 20 (red) mM Pi is modelled as a pseudo-first-order reaction. The experimental concentration of PhOH and cyclohexanone are shown as circles and squares, respectively. Best-fit lines are shown as solid and dashed curves, respectively. Results of the fit are shown in Table 1. (c) The rate of PhOH hydrogenation (k) is plotted *versus* the concentration of PhOH bound to the support determined by scNMR. Circles and squares are the data measured for the Pd/TiO_2 (this work) and Pd/CeO_2 (Egner *et al.*, 2020)[5] catalysts, respectively. Data obtained in the presence of 0 and 20 mM Pi are colored blue and red, respectively.

probability that the hydrogen bonded PhOH is located nearby Pd, Fig. 1). However, the data presented in Fig. 6c clearly indicate that similar concentrations of PhOH–support adduct result in similar conversion rates irrespective of the metal oxide used as the support (for example, compare the data reported for Pd/TiO_2 at 0 mM Pi to the ones measured for Pd/CeO_2 at 20 mM Pi in Fig. 6c).

A non-reducible support results in inefficient PhOH hydrogenation

To further test our hypothesis that hydrogen spillover is the main mechanism mediating hydrogenation of PhOH by Pd-supported on metal oxides, we have investigated the ability of Pd supported on Stöber silica (Pd/SiO_2) to adsorb and reduce PhOH. Silica (SiO_2) is a non-reducible support that is incapable to uptake Pd-activated hydrogen. Therefore, we expect Pd/SiO_2 to provide an inefficient catalyst for the PhOH hydrogenation reaction.

Pd/SiO_2 was prepared as described in methods. TEM images show that Pd/SiO_2 presents a spherical morphology with an average particle size of 22 ± 5 nm (Fig. 7a and Table 1). N_2 sorption analysis returned a catalyst surface area of 103.0 m^2 g^{-1}, and CO pulse chemisorption reported a 38.0% dispersion for Pd. The Pd particle size was calculated to be ~2.4 nm, and the metallic surface area was 1.4 m^2 g^{-1}. Therefore, the actual SiO_2 surface area on the catalyst is calculated as 101.6 m^2 g^{-1} (103.0–1.4 m^2 g^{-1}) (Table 1).

To confirm that hydrogen spillover does not occur in Pd/SiO_2, the SiO_2 and TiO_2 supports as well as the Pd/SiO_2 and Pd/TiO_2 catalysts were incubated under a flow of H_2 gas at 100 °C

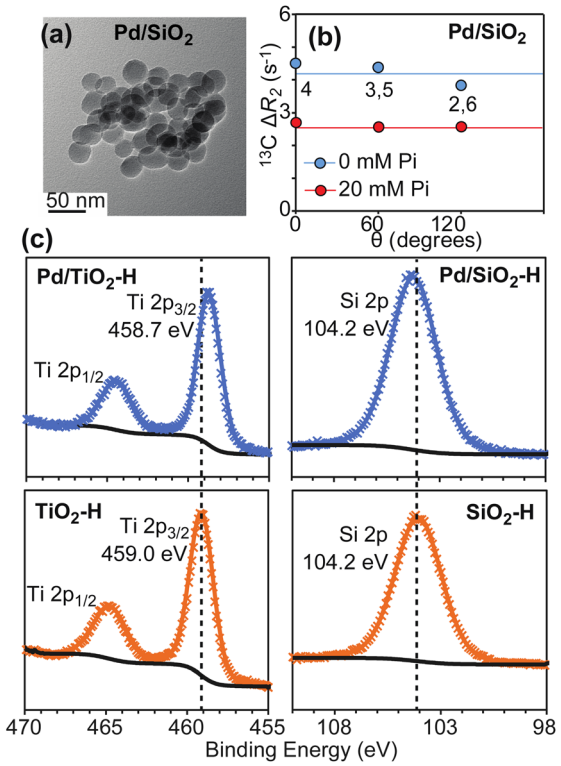

Fig. 7 Properties of Pd/SiO_2. Panel (a) shows a TEM image for the investigated Pd/SiO_2 material. Panel (b) shows a plot of the ^{13}C ΔR_2 as a function of θ measured for PhOH in the presence of 1 wt% Pd/SiO_2. The *ortho* (2,6) and *meta* (3,5) positions generate equivalent NMR peaks and one single ΔR_2 value for these peaks is reported. Data measured in the presence of 0 and 20 mM Pi are shown as blue and red spheres, respectively. Solid blue and red lines are the corresponding average ΔR_2 values. Panel (c) shows XPS spectra measured for TiO_2 (bottom left), Pd/TiO_2 (top left), SiO_2 (bottom right), and Pd/SiO_2 (top right) after hydrogen treatment (see ESI Methods†). The shift of the XPS Ti 2p peaks after hydrogen treatment is consistent with Ti reduction in the presence of supported Pd.

for 2 hours. The H_2 treated samples (SiO_2–H, TiO_2–H, Pd/SiO_2–H, and Pd/TiO_2–H, respectively) were then analyzed by X-ray Photoelectron Spectroscopy (XPS) without air exposure. The XPS spectra reported in Fig. 7c show that deposition of Pd on SiO_2 does not shift the Si 2p peak after H_2 treatment at 100 °C, which indicates that Si has the same oxidation state in SiO_2–H and Pd/SiO_2–H. On the other hand, comparison of the XPS spectra measured for Pd/TiO_2–H and TiO_2–H clearly indicates that the presence of Pd causes a negative shift of the Ti 2p binding energy by ~0.3 eV, which is consistent with spillover of Pd-activated hydrogen on the support and consequent reduction of the Ti sites. In this respect, it is important to notice, that deposition of Pd on TiO_2 does affect the oxidation of Ti intrinsically under reduction conditions, as evidenced by the fact that the XPS data measured for Pd/TiO_2 before H_2 treatment (Pd/TiO_2–I) and for TiO_2–H display Ti $2p_{3/2}$ peaks at the same binding energy (459.0 eV, ESI Fig. S3†).

Next, we investigated the ability of Pd/SiO_2 to adsorb PhOH on the support by ^{13}C ΔR_2 experiments. Analysis of the NMR data indicates that PhOH is efficiently adsorbed on Pd/SiO_2 (average $\Delta R_2 = 4.2 \pm 0.1$ s^{-1}, Fig. 7b and Table 1) and that addition of 20 mM Pi results in significant reduction in ΔR_2 (average $\Delta R_2 = 2.6 \pm 0.1$ s^{-1}, Fig. 7b and Table 1). In analogy to what reported above for Pd/TiO_2 and previously for Pd/CeO_2,[4,5] this ΔR_2 trend indicates formation of SiO_2–PhOH interactions that are destabilized by addition of Pi.

Finally, we established if Pd/SiO_2 can function as a catalyst for PhOH hydrogenation under the mild conditions tested for Pd/TiO_2 and Pd/CeO_2 (1 wt% catalyst, 1 bar of H_2, and 35 °C). Interestingly, no signs of substrate degradation or formation of hydrogenated products were detected after 12 hour incubation of Pd/SiO_2 with 10 mM PhOH (Table 1), confirming that the latter material is a worse hydrogenation catalyst than Pd/TiO_2. Of note, these results cannot be ascribed to different oxidation states of the Pd site in Pd/SiO_2 and Pd/TiO_2. Indeed, XPS data measured for these materials indicate that palladium deposits as metallic Pd on both metal oxides (ESI Fig. S3†). Therefore, we concluded that the low PhOH hydrogenation rate obtained with Pd/SiO_2 originates by its inability to uptake Pd-activated H_2 *via* spillover.

Conclusion

The outcome of a catalytic reaction is strictly dependent on the interactions that substrates, intermediates, and products form with the catalyst. Therefore, understanding how the kinetics and thermodynamics of adsorption regulate the efficiency of heterogeneous catalysts is of paramount importance in the design and optimization of catalytic processes. In this work, we have combined scNMR and reaction kinetics experiments to investigate how the structure, dynamics, and thermodynamic partitioning of the surface adsorbed species determine the PhOH hydrogenation reaction catalyzed by Pd/TiO_2. We showed that PhOH forms a weak interaction with the TiO_2 support that can be destabilized by the addition of 20 mM Pi. Interestingly, we noticed that the rate of PhOH hydrogenation is directly correlated to the amount of substrate adsorbed on titania (*i.e.*, a ~2-fold reduction in the concentration of adsorbed PhOH resulted in a ~2-fold reduction in catalytic conversion) (Table 1), indicating direct participation of the substrate–support interaction in catalysis.

In analogy with what we have previously observed for the adsorption of phenolic compounds on ceria nanoparticles, the formation of the catalytically competent PhOH–titania interaction likely involves the establishment of a hydrogen bond between the –OH group of the small molecule and one oxygen on the nanoparticle.[3–5,22] Consistent with this hypothesis, the S^2 modelled for the PhOH–titania adduct based on scNMR data is $\ll$0.1, which agrees well with the S^2 predicted for the C–H group of an aromatic ring connected to a rigid surface by three rotatable bonds.[5,16] Interestingly, the high conformational freedom of the adsorbed PhOH allows the substrate to adopt configurations in which the aromatic ring is adjacent to the surface of the heterogeneous catalyst and ideally positioned for the addition of activated hydrogens on the aromatic ring (Fig. 1a and 3a). In this respect, a comparison of the data measured on Pd/TiO_2 (this work) and Pd/CeO_2 (Egner *et al.* 2020)[5] revealed

that the rate of the PhOH hydrogenation reaction is directly correlated to the amount of PhOH hydrogen bonded to the metal oxide support (Fig. 6c). Since titania and ceria have similar abilities to uptake hydrogen activated by a supported noble metal,[10] our data suggest that hydrogen spillover on the support is the main mechanism by which the Pd-activated hydrogen is shuttled to the PhOH hydrogen bonded to the metal oxide support. The latter conclusion is consistent with the fact that strong Pd–substrate interactions were observed to inhibit the rate of hydrogenation of 2-hydroxy- and 2-methoxy-PhOH,[4] and that using a support that does not mediate hydrogen spillover such as silica results in inefficient hydrogenation catalysis. Overall, the results presented in this work indicate that ceria provides the ideal support for the PhOH hydrogenation reaction thanks to its redox properties that permit spillover of the activated hydrogen and to its basic properties that facilitate the establishment of the catalytically competent substrate–support hydrogen bonding interaction.

Experimental methods

Synthesis of Pd/TiO_2

25 mg of palladium(II) nitrate dihydrate from Sigma-Aldrich was dissolved in *ca.* 500 μL deionized water. 1 g of titanium(IV) oxide nanopowder (anatase, <25 nm particle size) from Aldrich was impregnated with the Pd precursor solution by incipient wetness method targeting 1 wt% Pd loading. The catalyst was then dried under vacuum and reduced under H_2 flow (15 cm^3 min^{-1}) for 2 h at 100 °C. The reduction temperature was kept under 100 °C to prevent the formation of a TiO_x layer on the Pd surface.[23]

Synthesis of Pd/SiO_2

Silica nanoparticles were synthesized following the Stöber method. Briefly, in a 250 mL round-bottom flask, 190 mL ethanol was mixed with 10 mL DI water, followed by the addition of ~3.75 mL concentrated ammonium hydroxide solution. The mixture was stirred at 550 rpm and 40 °C for ~1 h. Then, ~2.5 mL of tetraethylorthosilicate (TEOS) was added to the mixture and stirred for 24 h at 40 °C. The material was filtered with thorough washing by ethanol followed by drying at 100 °C overnight to obtain ~0.5 g of dry silica powder. The Pd/SiO_2 catalyst was synthesized following the protocol described above for preparations of Pd/TiO_2.

Transmission electron microscopy

TiO_2 and Pd/TiO_2 nanoparticles were imaged in a FEI Tecnai G2 F20 field emission transmission electron microscope (TEM) operating at 200 kV. Samples were prepared by placing 3–4 drops of ethanol suspension (~0.1 mg mL^{-1}) onto lacey-carbon-coated copper grids and dried in air. Size distribution histograms and average particle size were obtained from TEM images by measuring the diameter of 100 particles using the Digital Micrograph® software.

Inductively coupled plasma-optical emission spectroscopy (ICP-OES)

Pd loadings were measured in a PerkinElmer Optima 2100 DV ICP-OES instrument. Samples (10 mg) were sonicated and vortexed for 24 h in 2 mL *aqua regia*. The solution was diluted to 12.0 mL using deionized water (17.4 Mohm cm). The solution was filtered and the amount of palladium in the filtrate was determined by comparing the ICP-OES signal with the signal obtained from calibration standards.

Surface area measurements

Specific surface areas of the materials were calculated from N_2 sorption isotherms measured in a Micromeritics Tristar Analyzer at −196 °C. Prior to the measurement, the samples were pretreated at 100 °C for 6 h under N_2 flow. The specific surface areas of the materials were calculated using the Brunauer–Emmett–Teller (BET) method.

CO pulse chemisorption

Micromeritics Autochem II 2920 Chemisorption Analyzer was used for the CO pulse chemisorption. A glass wool bed was inserted in a quartz U-tube, and 100 mg of Pd/TiO_2 was loaded on top of the wool. The catalyst was then reduced under H_2 flow (10% in Ar) at a flow rate of 30 cm^3 min^{-1} for 60 min at 100 °C, followed by treatment with a He flow (flow rate: 50 cm^3 min^{-1}) for 30 min at 100 °C to remove excess surface bonded H atoms. The temperature was then lowered to 40 °C under the same He flow and held for 30 min. The catalyst was then subjected to CO pulses (10% in He). The palladium dispersion and surface area were calculated as described in ESI Methods.†

XPS sample preparation and experiments

A clean oven-dried flat-bottomed Schlenk flask (100 mL) was cooled under vacuum and then cycled with UHP hydrogen. Then under a heavy purge of hydrogen, the sample was introduced into the flask, and the vacuum was pulled. The sample was kept in a vacuum at 100 °C for 30 min to ensure complete removal of surface moisture. Then hydrogen was flowed at 15 cm^3 min^{-1} for 2 h at 100 °C. The color of the Pd-impregnated samples darkened over time. At the end of 2 h, the flask was cooled under hydrogen flow, sealed, and introduced into a dry glove box. The reduced samples were stored in a glass-on-glass sample storage tube until further use. The samples after this treatment were named TiO_2–H, Pd/TiO_2–H, SiO_2–H, and Pd/SiO_2–H, respectively. All these samples were loaded in the air-free XPS chamber directly from the glovebox to ensure no surface reoxidation takes place during handling. XPS data on the on TiO_2, Pd/TiO_2, SiO_2, and Pd/SiO_2 before and after H_2 treatment were acquired using a Kratos Amicus XPS system. The XPS data were modelled using the CasaXPS software.

Hydrogenation of phenol

10 mM PhOH solutions were prepared in deionized water (17.4 Mohm cm), and 20 mM phosphate buffer, respectively, and the pH was adjusted to 7.0 ± 0.1 using dilute HCl or NaOH. In

a typical reaction, the catalyst (20 mg, 5 mol%) and PhOH solution (4 mL, 10 mM) were added to a 10 mL glass tube. The tube was sealed and purged with H_2 for 10 min at a rate of 20 cm^3 min^{-1}. After 10 min, the pressure relief needle was removed, and the H_2 supply was stopped. The reaction tube was then placed in an oil bath preset at 35 °C under constant stirring (800 rpm). After the desired time, the septum was removed, and the catalyst was separated by centrifugation. The solution was extracted 4 times with 1 mL ethyl acetate. A 50 μL aliquot of the extracted solution was taken and analyzed by GC-MS (Agilent 7890A, 5975C) with an HP-5MS column, using 100 μL resorcinol (55 mM) as internal standard. The run started at 60 °C, the temperature was then ramped to 150 °C at 5 °C min^{-1}, then to 300 °C at a ramp of 20 °C min^{-1} and finally held constant at 300 °C for 3 min. The reaction kinetic data were analyzed assuming a pseudo-first-order reaction. The time dependency of the concentrations of PhOH and cyclohexanone are given by:

$$[\mathrm{PhOH}] = [\mathrm{PhOH}]_0 e^{-kt} \quad (1)$$

$$[\mathrm{Cyclohexanone}] = [\mathrm{PhOH}]_0(1 - e^{-kt}) \quad (2)$$

where $[PhOH]_0$ is the initial concentration of PhOH, k is the pseudo-first-order reaction rate, and t is the time. The experimental error was determined by running three replicas of the hydrogenation reaction. Error on the fitted rate was computed by Monte Carlo simulation of synthetic datasets from the estimated experimental error. The fitted k has a unit of M s^{-1} since it depends on the concentration of catalytic sites in the reaction mixture.

Preparation of the NMR samples

Nanoparticle suspensions were prepared in an agarose gel matrix, as previously described.[22] The pH of the phenol solution (10 mM) prepared in D_2O was adjusted to 7.0 ± 0.1 using dilute DCl or NaOD. The pH was read directly from the pH meter without correction for isotope effects. Then nanoparticles (1 wt%) and agarose (1 wt%) were added to the solution. For the samples prepared in the presence of phosphate, sodium phosphate was added to a 20 mM final concentration and pH adjusted to 7.0 ± 0.1 using dilute DCl or NaOD. The mixture was then sonicated for 1 min (1 : 2 on/off duty cycle) at 25% power on a 500 W horn-tipped sonicator, heated to 80 °C for 10 min, transferred to a 5 mm NMR tube, and allowed to cool at room temperature for 10–15 min. The reference samples that did not contain nanoparticles were prepared using the same procedures as above. Phenol and agarose were purchased from Sigma-Aldrich. DCl and NaOD were purchased from Cambridge Isotope Laboratories. All chemicals were used without further purification.

NMR spectroscopy

^{13}C R_2 NMR data were collected at 25 °C on Bruker 400 and 800 MHz spectrometer equipped with triple resonance z-gradient cryoprobes. ^{13}C R_2 was measured using a double INEPT-based CPMG sequence with proton decoupling during the ^{13}C relaxation period.[5] The ^{13}C carrier frequency was set at the center of the three peaks of the aromatic ring in PhOH. The CPMG field strength was set to 1 kHz. 14 different relaxation delays were acquired in an interleaved manner to obtain the ^{13}C R_2 relaxation decay curve. The observed relaxation decay was fitted using a monoexponential decay function ae^{-R_2t}, where a is the scaling factor, R_2 is the transverse relaxation rate, and t is the variable relaxation delay. The experiments were acquired with 32 dummy scans and 128 scans with a recycle delay of 4 s between each scan. NMR spectra were processed and analyzed using the Mnova NMR software (**https://mestrelab.com/software/mnova/nmr/**).

^{13}C DEST, ^{13}C RD, and ^{13}C R_1 NMR data were collected at 25 °C on Bruker 400, 600, and 800 MHz spectrometers equipped with triple resonance z-gradient cryoprobes and using the pulse sequences shown in the literature.[5] Details on the NMR data acquisition and analysis are provided in ESI Methods.†

Data availability

All data are available upon request.

Author contributions

Y. A., P. C., P. N., S. B. and V. V. designed and performed the research; Y. A., P. C., W. H., I. I. S. and V. V. analyzed the data; Y. A., P. C. and V. V. wrote the manuscript; W. H., I. I. S. and V. V. acquired funding for the project.

Conflicts of interest

The authors declare no conflict of interest.

Acknowledgements

This work was supported by funds from the National Institute of General Medical Sciences with grant no. R35GM133488 (to V.V.), and by the U.S. Department of Energy, Office of Basic Energy Sciences, Division of Chemical Sciences, Geosciences, and Biosciences, through the Ames Laboratory Catalysis Science Program (to I. I. S.). The Ames Laboratory is operated for the U.S. Department of Energy by Iowa State University under contract no. DE-AC02-07CH11358. W. H. acknowledges support from National Science Foundation grant CHE-2108307.

References

1 M. Weber, M. Weber and M. Kleine-Boymann, in *Ullmann's Encyclopedia of Industrial Chemistry*, Wiley-VCH Verlag GmbH & Co. KGaA, 2000.
2 M. T. Musser, in *Ullmann's Encyclopedia of Industrial Chemistry*, Wiley-VCH Verlag GmbH & Co. KGaA, 2000.
3 N. C. Nelson, J. S. Manzano, A. D. Sadow, S. H. Overbury and I. I. Slowing, *ACS Catal.*, 2015, **5**, 2051–2061.
4 Y. An, P. Naik, I. I. Slowing and V. Venditti, *ACS Appl. Nano Mater.*, 2020, **3**, 11282–11288.
5 T. K. Egner, *et al.*, *ChemCatChem*, 2020, **12**, 4160–4166.

6 P. J. Naik, *et al.*, *ACS Catal.*, 2021, **11**, 10553–10564.
7 Y. An, S. L. Sedinkin and V. Venditti, *Nanoscale Adv.*, 2022, **4**, 2583–2607.
8 D. Zhang, F. Ye, T. Xue, Y. Guan and Y. M. Wang, *Catal. Today*, 2014, **234**, 133–138.
9 H. Zhou, *et al.*, *Green Chem.*, 2017, **19**, 3585–3594.
10 A. Beck, *et al.*, *J. Phys. Chem. C*, 2022, **126**, 17589–17597.
11 N. Pineda-Aguilar, L. L. Garza-Tovar, E. M. Sánchez-Cervantes and M. Sánchez-Domínguez, *J. Mater. Sci.: Mater. Electron.*, 2018, **29**, 15464–15479.
12 C. Z. Wen, H. B. Jiang, S. Z. Qiao, H. G. Yang and G. Q. Lu, *J. Mater. Chem.*, 2011, **21**, 7052–7061.
13 R. Liang, A. Hu, J. Persic and Y. N. Zhou, *Nano-Micro Lett.*, 2013, **5**, 202–212.
14 L. Wu, D. Buchholz, D. Bresser, L. Gomes Chagas and S. Passerini, *J. Power Sources*, 2014, **251**, 379–385.
15 M. Xie and R. Bruschweiler, *J. Phys. Chem. Lett.*, 2020, **11**, 10401–10407.
16 J. R. Sachleben, V. Colvin, L. Emsley, E. W. Wooten and A. P. Alivisatos, *J. Phys. Chem. B*, 1998, **102**, 10117–10128.
17 E. T. Kho, S. Jantarang, Z. Zheng, J. Scott and R. Amal, *Engineering*, 2017, **3**, 393–401.
18 X. Wang, B. Liu and J. Liu, *Langmuir*, 2018, **34**, 15871–15877.
19 R. R. Dotas, *et al.*, *J. Mol. Biol.*, 2020, **432**, 4481–4498.
20 R. Ghose, *J. Mol. Biol.*, 2019, **431**, 145–157.
21 H. P. Lu, L. Xun and X. S. Xie, *Science*, 1998, **282**, 1877–1882.
22 T. K. Egner, P. Naik, N. C. Nelson, I. I. Slowing and V. Venditti, *Angew. Chem., Int. Ed.*, 2017, **56**, 9802–9806.
23 S. Zhang, *et al.*, *Nano Lett.*, 2016, **16**, 4528–4534.